Solid State Ionics 362 (2021) 115585

Contents lists available at ScienceDirect

Solid State Ionics

journal homepage: www.elsevier.com/locate/ssi

Lithium-ion diffusivity in complex hydrides: Pulsed-field-gradient NMR studies of $LiLa(BH_4)_3Cl$, $Li_3(NH_2)_2I$ and Li-1-CB_9H_{10}

A.V. Skripov [a,*], G. Majer [b], O.A. Babanova [a,c], R.V. Skoryunov [a], A.V. Soloninin [a], M.B. Ley [d], T. R. Jensen [d], S. Orimo [e,f], T.J. Udovic [g,h]

[a] Institute of Metal Physics, Ural Branch of the Russian Academy of Sciences, Ekaterinburg 620108, Russia
[b] Max-Planck-Institute for Intelligent Systems, 70569 Stuttgart, Germany
[c] Ural Federal University, Ekaterinburg 620002, Russia
[d] Interdisciplinary Nanoscience Center (iNANO), and Department of Chemistry, Aarhus University, DK-8000 Aarhus, Denmark
[e] Institute for Materials Research, Tohoku University, Sendai, 980-8577, Japan
[f] WPI-Advanced Institute for Materials Research, Tohoku University, Sendai 980-8577, Japan
[g] NIST Center for Neutron Research, National Institute of Standards and Technology, Gaithersburg, MD 20899-6102, USA
[h] Department of Materials Science and Engineering, University of Maryland, College Park, MD 20742, USA

ARTICLE INFO

Keywords:
Complex hydrides
Ionic conductors
Diffusion
Nuclear magnetic resonance

ABSTRACT

The bimetallic borohydride-chloride $LiLa(BH_4)_3Cl$, the lithium amide-iodide $Li_3(NH_2)_2I$, and the lithium monocarba-*closo*-decaborate Li-1-CB_9H_{10} represent complex hydrides showing superionic conductivity at room temperature or slightly above it. To study the Li-ion diffusivity that is closely related to the ionic conductivity, we have measured the diffusion coefficients of Li^+ cations in these compounds using the pulsed-field-gradient (PFG) spin-echo technique over the temperature range of 298–403 K. The experiments have revealed fast Li^+ diffusivities in all these complex hydrides: at 400 K, the measured diffusion coefficients exceed 10^{-7} cm^2/s for $LiLa(BH_4)_3Cl$, 5×10^{-8} cm^2/s for $Li_3(NH_2)_2I$, and 10^{-6} cm^2/s for Li-1-CB_9H_{10}. For $LiLa(BH_4)_3Cl$ and $Li_3(NH_2)_2I$, the diffusion coefficients are found to follow the Arrhenius behavior over the entire temperature ranges studied with the activation energies of 268(6) meV and 224(6) meV, respectively. For Li-1-CB_9H_{10}, the Arrhenius behavior with the activation energy of 265(6) meV is observed in the disordered high-temperature polymorph (360–403 K), whereas below 360 K the measured diffusivity drops significantly due to the transition to the ordered phase. Comparison of the measured Li^+ diffusion coefficients with the ionic conductivity results and the data on the cation and anion jump rates provides new insights into the unusual dynamical properties of these superionic materials.

1. Introduction

Complex hydrides described by the general formula $M_x[A_mH_n]_y$ are ionic compounds consisting of metal cations M and complex anions $[A_mH_n]$, such as $[BH_4]^-$, $[NH_2]^-$, $[AlH_4]^-$, $[SiH_3]^-$, $[B_{12}H_{12}]^{2-}$, or $[B_{10}H_{10}]^{2-}$. Due to high volumetric and gravimetric hydrogen densities, these compounds are considered as prospective materials for hydrogen storage [1,2]. Recently, it has been found that some complex hydrides also exhibit high ionic conductivity [3–10]. The archetypical example is lithium borohydride $LiBH_4$, in which the first-order phase transition from the low-T orthorhombic phase to the high-T hexagonal phase is accompanied by a three-orders-of-magnitude increase in Li-ion conductivity, so that the conductivity exceeds 10^{-3} S/cm above 390 K [3]. Another interesting class of complex hydrides showing high ionic conductivity is represented by lithium and sodium *closo*-hydroborates based on $[B_{12}H_{12}]^{2-}$ and $[B_{10}H_{10}]^{2-}$ anions and their modifications [8–11]. In particular, the carbon-substituted mixed-anion *closo*-hydroborate $Na_2(CB_9H_{10})(CB_{11}H_{12})$ is found to exhibit the highest room-temperature ionic conductivity (~0.07 S/cm [11]) among all the studied Na-ion and Li-ion conductors.

The important dynamical feature of complex hydrides is that complex anions can undergo fast reorientational (rotational) motion [12–15]. This motion strongly contributes to the balance of energies determining the thermodynamic stability. Furthermore, the anion reorientations may be related to the diffusive mobility of the cations. Indeed, a number of experimental studies have revealed that the fast

* Corresponding author.
E-mail address: skripov@imp.uran.ru (A.V. Skripov).

https://doi.org/10.1016/j.ssi.2021.115585
Received 30 November 2020; Received in revised form 3 February 2021; Accepted 17 February 2021
0167-2738/© 2021 Elsevier B.V. All rights reserved.

diffusive motion of the cations in complex hydrides is accompanied by the fast reorientational motion of the anions [9,10,13–15]. Recent ab initio molecular dynamics calculations suggest that reorientations of large icosahedral $[B_{12}H_{12}]^{2-}$ and related anions in lithium and sodium *closo*-hydroborates can facilitate cation mobility [16–19]. In order to elucidate the mechanisms of ionic conductivity in complex hydrides, it is important to obtain experimental information on both the reorientational motion of the anions and the diffusive mobility of the cations. Nuclear magnetic resonance (NMR) has proved to be an effective method for studies of atomic jump motion in solids at the microscopic level. In favorable cases, measurements of NMR spectra and nuclear spin relaxation rates can probe the atomic jump rates in complex hydrides over the range of eight orders of magnitude (10^4–10^8 s^{-1}) [20]. However, standard NMR and relaxation measurements cannot give direct information on diffusion coefficients of the cations. Yet, such information can be obtained using the pulsed-field-gradient (PFG) spin-echo NMR technique [21–24]. This technique employs an external magnetic field gradient to set a spatial scale of atomic motion in a certain direction, and thus provides a bridge between microscopic and macroscopic measurements of ionic mobility. Combining the direct PFG-NMR measurements of diffusion coefficients with the nuclear spin relaxation measurements of atomic jump rates, it is in principle possible to obtain information on the diffusion path. Therefore, such a combination is crucial for understanding the diffusion mechanism. To the best of our knowledge, the only PFG-NMR study of Li^+ diffusivity in complex hydrides was recently reported for the mixed-anion system $Li(CB_9H_{10})_{0.7}(CB_{11}H_{12})_{0.3}$ [25], and the first PFG-NMR measurements of Na^+ diffusivity in complex hydrides were reported for Na-7-$CB_{10}H_{13}$ and $Na_2(CB_9H_{10})(CB_{11}H_{12})$ [26].

In this work, we present the results of PFG-NMR measurements of the temperature dependences of Li^+ diffusivity in three complex hydrides, in which previous nuclear spin relaxation measurements revealed high lithium mobility at room temperature or slightly above it [10,27–29]: $LiLa(BH_4)_3Cl$, $Li_3(NH_2)_2I$, and Li-1-CB_9H_{10}. (The latter formula indicates that a carbon atom substitutes the *apical* boron in the bicapped-square-antiprismatic cage; in the following, this compound will be more simply referred to as $LiCB_9H_{10}$). The bimetallic borohydride-chloride $LiLa(BH_4)_3Cl$ consists of isolated anionic clusters $[La_4Cl_4(BH_4)_{12}]^{4-}$ with the distorted cubane La_4Cl_4 core, charge-balanced by Li^+ cations [7]. The Li^+ jump rate in this compound estimated from the nuclear spin-lattice relaxation measurements [27] reaches ~10^8 s^{-1} at room temperature. Furthermore, this is the first borohydride-based system where Li^+ jump motion and a certain type of $[BH_4]^-$ reorientations are found to occur *at the same frequency scale* [27]. In lithium amide-iodide $Li_3(NH_2)_2I$, the Li^+ jump rate also reaches 10^8 s^{-1} near room temperature [28]. The most interesting feature of lithium monocarba-*closo*-decaborate $LiCB_9H_{10}$ is the order-disorder phase transition occurring near 360 K; this transition is accompanied by a dramatic increase in the ionic conductivity reaching ~0.1 S/cm at 383 K [10]. According to NMR and quasielastic neutron scattering (QENS) results [10,30], in the high-temperature disordered phase of $LiCB_9H_{10}$, the reorientational jump rate of the polyhedral (bicapped-square-antiprismatic) $[CB_9H_{10}]^-$ anions exceeds 10^{10} s^{-1}, and the diffusive jump rate of Li^+ cations considerably exceeds 10^8 s^{-1}.

2. Experimental details

The preparation of $LiLa(BH_4)_3Cl$ was analogous to that described in Ref. [7]. All preparation and manipulation procedures were performed in an argon-filled glovebox. A $LaCl_3$ – $LiBH_4$ mixture with 1:3 molar ratio was ball-milled in a Fritsch Pulverisette 4 planetary mill [31] in an argon atmosphere using tungsten carbide balls and vial with 1:35 sample-to-balls mass ratio. To minimize sample heating, a 2 min milling period was followed by 2 min pause, and this procedure was repeated 60 times. After the milling, the sample was annealed at 473 K for 30 min under H_2 (10 bar) atmosphere. According to X-ray diffraction analysis, the resulting sample consisted of cubic $LiLa(BH_4)_3Cl$ (space group $I\bar{4}3m$, a = 11.7955(1) Å) and LiCl. The preparation of $Li_3(NH_2)_2I$ was analogous to that described in Ref. [6]. All preparation and manipulation procedures were performed in a glovebox filled with purified argon. A $LiNH_2$ – LiI mixture (3:1 molar ratio) was mechanically milled for 5 h in an argon atmosphere using a planetary Fritsch 7 ball mill at 400 rpm. After the milling, the sample was heat-treated at 423 K for 12 h under argon. According to X-ray diffraction analysis, the major phase of the resulting sample was hexagonal $Li_3(NH_2)_2I$ (space group $P6_3mc$, a = 7.09109(5) Å, c = 11.50958(10) Å). The sample also contained unreacted $LiNH_2$ as a minor phase. Lithium 1-monocarba-*closo*-decaborate $LiCB_9H_{10}$ was obtained from Katchem, and the residual water was removed by annealing in vacuum overnight at 473 K. According to X-ray diffraction analysis, the high-temperature disordered phase of $LiCB_9H_{10}$ at 383 K is hexagonal (space group $P3_1c$, a = 6.829 Å, c = 10.754 Å). Moreover, there is an intermediate partially disordered orthorhombic phase at 333 K (space group $Cmc2_1$, a = 6.807 Å, b = 11.819 Å, c = 10.604 Å), and an ordered phase exists below 320–330 K [10]. For NMR experiments, the samples were flame-sealed in glass tubes under 500 mbar of nitrogen gas ($LiLa(BH_4)_3Cl$) or under vacuum ($Li_3(NH_2)_2I$ and $LiCB_9H_{10}$).

Measurements of the ^1H and ^7Li NMR spectra were performed on a pulse spectrometer with quadrature phase detection at the frequency $\omega/2\pi$ = 28 MHz. The magnetic field was provided by a 2.1 T iron-core Bruker magnet. A home-built multinuclear continuous-wave NMR magnetometer working in the range 0.32–2.15 T was used for field stabilization. For rf pulse generation, we used a home-built computer-controlled pulse programmer, the PTS frequency synthesizer (Programmed Test Sources, Inc.), and a 1 kW Kalmus wideband pulse amplifier. Typical values of the $\pi/2$ pulse length were 2–3 μs. A probehead with the sample was placed into an Oxford Instruments CF1200 continuous-flow cryostat using nitrogen as a cooling agent. The sample temperature, monitored by a chromel-(Au—Fe) thermocouple, was stable to ±0.1 K. NMR spectra were recorded by Fourier transforming the solid echo signals (pulse sequence $\pi/2 - t - \pi/2_y$).

Pulsed-field-gradient NMR (PFG-NMR) measurements of Li^+ diffusion coefficients were performed on a Bruker AVANCE III 400 spectrometer operating at the resonance frequency of 155.4 MHz. Magnetic field gradients were generated by a diff60 diffusion probe and a Great60 gradient amplifier (Bruker Biospin). All ^7Li diffusivities were measured using the stimulated echo sequence [32]. The shape of the gradient pulses was given by a half-sine function with a length of δ_{sine}, which corresponds to the effective gradient pulse length of $\delta_g = (2/\pi)\delta_{sine}$. The diffusion coefficients were deduced from the decrease in the integrated intensity of Fourier-transformed spin-echo with increasing amplitude of the applied field-gradient pulses g. The diffusion time Δ between two gradient pulses of the pulse sequence was between 10 ms and 30 ms, and their effective length δ_g was between 1 ms and 2 ms. The amplitude of the gradient pulses g was varied in 16 steps up to 2.9 kG/cm.

For all figures, standard uncertainties are commensurate with the observed scatter in the data, if not explicitly designated by vertical error bars.

3. Results and discussion

For sinusoidal field-gradient pulses, the diffusion-induced attenuation of the spin-echo intensity A as a function of the pulsed field gradient amplitude g can be written in the form [23,33,34].

$$\frac{A(g)}{A(0)} = exp\left[-\gamma^2 D\delta_g^2\left(\Delta - \frac{\pi}{8}\delta_g\right)g^2\right], \quad (1)$$

where D is the diffusion coefficient, γ is the gyromagnetic ratio for ^7Li, and δ_g is the effective gradient pulse length. As an example of the data, Fig. 1 shows the spin-echo attenuation as a function of g^2 for $LiCB_9H_{10}$ at three temperatures. It evident from this figure that logarithm of $A(g)$ scales linearly with g^2, as expected from Eq. (1). Similar behavior of the

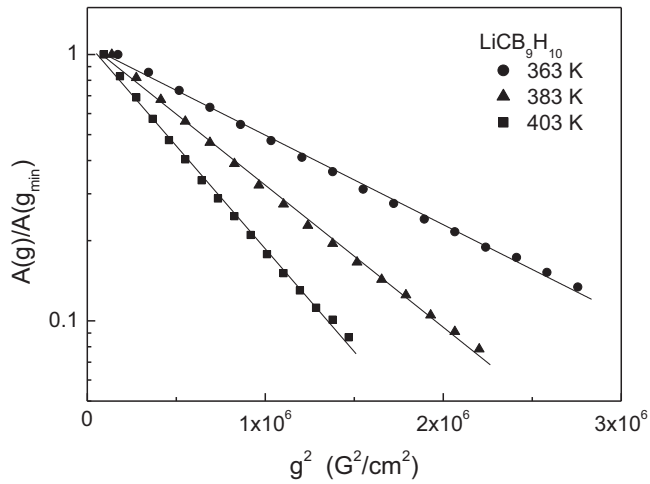

Fig. 1. The ^{7}Li spin-echo amplitude normalized to the amplitude measured with the smallest gradient as a function of the square of the effective gradient pulse amplitude for $LiCB_9H_{10}$ at three temperatures. The solid lines show the nonlinear least-squares regressions of Eq. (1) to the data.

spin-echo attenuation was also observed for $LiLa(BH_4)_3Cl$ and $Li_3(NH_2)_2I$ (see Figs. S1 and S2 of the Supplementary Information).

3.1. Li^+ diffusivity in $LiLa(BH_4)_3Cl$

The Li^+ diffusion coefficients derived from the spin-echo attenuation for $LiLa(BH_4)_3Cl$ and $Li_3(NH_2)_2I$ are shown in Fig. 2 as functions of the inverse temperature. For both compounds, the high values of the measured Li^+ diffusivity are consistent with the results of previous ^{7}Li NMR measurements of the spectra and spin-lattice relaxation rates [27–29]. In particular, for $LiLa(BH_4)_3Cl$, the step-like narrowing of the ^{7}Li NMR line was observed near 230 K, and the ^{7}Li spin-lattice relaxation rate maximum at 28 MHz was found near 297 K [27]. As can be seen from Fig. 2, the Li^+ diffusivity in $LiLa(BH_4)_3Cl$ exhibits the Arrhenius-type behavior over the temperature range of 298–403 K. The corresponding activation energy derived from the Arrhenius fit of the $D(T)$ data is 268(6) meV. This value is close to the rough estimate of the activation energy for Li^+ diffusion obtained from the high-temperature slope of the ^{7}Li spin-lattice relaxation rate peak (~ 300 meV [27]). Furthermore, this value is very close to the activation energy for the slowest process of $[BH_4]^-$ reorientations occurring at the same frequency scale as Li^+ diffusive jumps (264(8) meV [27]). Since the activation energies obtained from the PFG-NMR measurements of Li^+ diffusivity and from the relaxation rate measurements of Li^+ jump rates are close to each other, we may assume that they are governed by the same diffusive process; this forms a basis for an estimate of the elementary jump length L. Neglecting any correlations for diffusive jumps, L can be estimated from the expression $D = L^2\tau^{-1}/6$, where τ^{-1} is the jump rate of lithium ions. Using the experimental values of D(297 K) $= 7.69 \times 10^{-9}$ cm^2/s and τ^{-1}(297 K) $\approx 1.8 \times 10^8$ s^{-1} at the ^{7}Li spin-lattice relaxation rate maximum [27], we obtain $L = 1.6$ Å.

In the original structural model of $LiLa(BH_4)_3Cl$ [7], Li^+ ions were proposed to occupy randomly 2/3 of the available 12*d* interstitial sites coordinated by four $[BH_4]^-$ groups. The sublattice of 12*d* sites (see Fig. 3) can be considered favorable for diffusive motion [27]. However, the distance l_{dd} between the nearest-neighbor 12*d* sites in $LiLa(BH_4)_3Cl$ is 4.17 Å, which is considerably larger than the value of L estimated from the diffusivity experiments. It should be noted that a recent study of the Li^+ diffusion mechanism in the related $LiCe(BH_4)_3Cl$ compound based on first-principles calculations [35] has revealed that the Li ion jumps to the nearest 12*d* site indirectly by passing through the nearest 6*b* site (the tetrahedral interstitial 6*b* sites are also included in Fig. 3). Furthermore, the 6*b* site appears to be an additional stable Li ion site, and a partial occupancy of the 6*b* sites by Li ions in $LiCe(BH_4)_3Cl$ is consistent with the results of the diffraction experiments [35].

Since $LiLa(BH_4)_3Cl$ and $LiCe(BH_4)_3Cl$ have the same structures with only slightly differing lattice parameters [7,36,37], it is reasonable to assume that the tetrahedral 6*b* sites are also partially occupied by Li ions in $LiLa(BH_4)_3Cl$, and the Li^+ diffusion mechanisms in these compounds are the same. The distance l_{db} between the nearest-neighbor 12*d* and 6*b* sites in $LiLa(BH_4)_3Cl$ is 2.95 Å, which is considerably shorter than l_{dd} and closer to the estimated jump length L. Moreover, if we take into account the tracer correlation factor f (which, depending on the geometry of diffusion paths, can be between 0 and 1), the jump length estimated from the comparison of D and τ^{-1} may become longer. For example, for

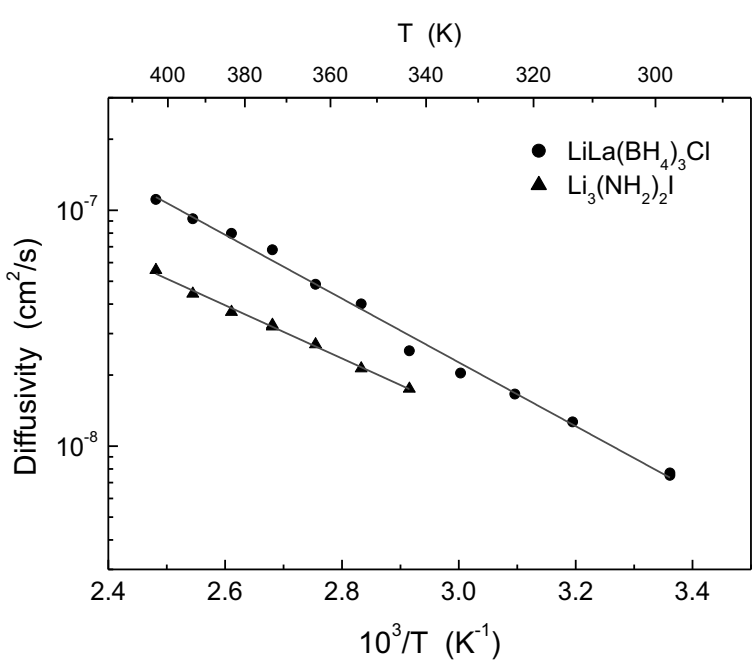

Fig. 2. The measured Li^+ diffusion coefficients for $LiLa(BH_4)_3Cl$ and $Li_3(NH_2)_2I$ as functions of the inverse temperature. The red lines show the Arrhenius fits to the data. (For interpretation of the references to colour in this figure legend, the reader is referred to the web version of this article.)

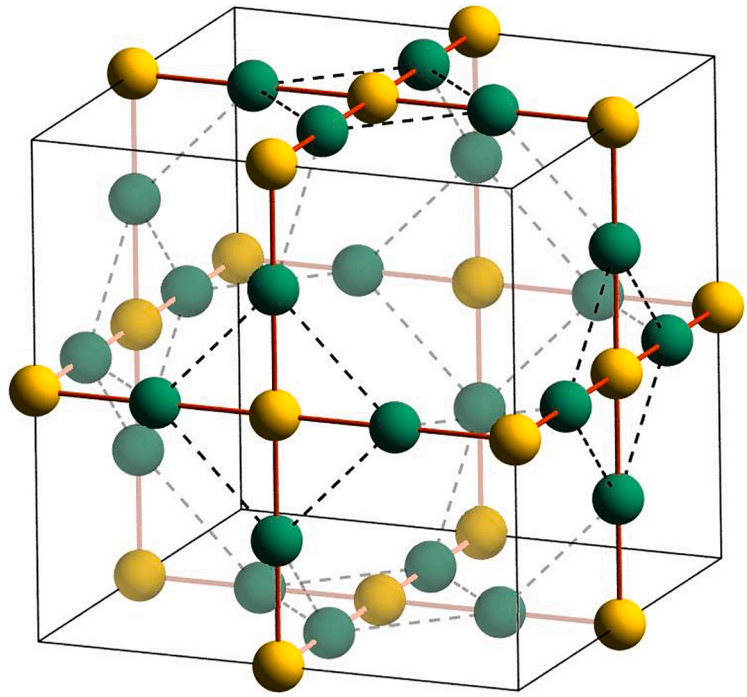

Fig. 3. The sublattice of 12*d* sites (green spheres) and 6*b* sites (yellow spheres) partially occupied by Li ions in $LiLa(BH_4)_3Cl$. Dashed lines connect the nearest-neighbor 12*d* sites. Red bars show the possible diffusion paths within the unit cell. (For interpretation of the references to colour in this figure legend, the reader is referred to the web version of this article.)

a realistic value of $f = 0.5$, we would obtain $L = 2.3$ Å. Thus, it can be concluded that the preferable Li^+ diffusion mechanism in $LiLa(BH_4)_3Cl$ includes jumps between 12*d* and 6*b* sites (see Fig. 3). Another possible approach to verify 12*d* – 6*b* jumps may be related to using spin-alignment echo (SAE) NMR spectroscopy [38–40]. This technique employs nuclear quadrupole frequencies to label the diffusing ions; in principle, it can distinguish between different diffusion paths [39,40].

Since Li^+ jumps and a certain type of BH_4^- reorientations in $LiLa(BH_4)_3Cl$ occur at the same frequency scale [27], they may be correlated. It should be stressed that such a conclusion is based on the analysis of the amplitude of the ^1H spin-lattice relaxation rate peak, not just on the fact that the ^1H and ^7Li relaxation rate peaks are observed at nearly the same temperatures [27]. Indeed, the amplitude of the ^1H spin-lattice relaxation rate peak near room temperature is found to be much higher than that expected solely due to modulation of the ^1H – ^7Li dipole-dipole interaction in $LiLa(BH_4)_3Cl$ [27].

The measured tracer diffusion coefficient can be used to estimate the ionic conductivity σ from the Nernst-Einstein equation

$$\sigma = \frac{nD(Ze)^2}{k_B T}, \tag{3}$$

where n is the number of charge carriers per unit volume and Ze is the electrical charge of the carrier. Using the lattice parameter of $LiLa(BH_4)_3Cl$ [7], we find that $n = 4.88 \times 10^{21}$ cm^{-3} and $\sigma(297\ K) \approx 2.4 \times 10^{-4}$ S/cm. This value is in agreement with the measured room-temperature ionic conductivity of $LiLa(BH_4)_3Cl$ (2.3×10^{-4} S/cm) [7]. It should be noted, however, that the measured ionic conductivity depends on the purity of $LiLa(BH_4)_3Cl$ samples (which can be synthesized by different methods) and on the type of electrodes used in the measurements [41]. In particular, $LiLa(BH_4)_3Cl$ samples are known to contain the impurity LiCl phase with very poor ionic conductivity [7,41]. The activation energy for the ionic conductivity measured on the purest $LiLa(BH_4)_3Cl$ sample is 307 meV [41], which is close to the activation energy for Li^+ diffusivity obtained in the present work.

3.2. Li^+ diffusivity in $Li_3(NH_2)_2I$

As can be seen from Fig. 2, in the studied temperature range, the diffusion coefficient of Li^+ in $Li_3(NH_2)_2I$ is somewhat lower than that in $LiLa(BH_4)_3Cl$. The Arrhenius approximation of the $D(T)$ data for $Li_3(NH_2)_2I$ over the range of 343–403 K gives the activation energy of 224(6) meV. In the previous NMR relaxation study of $Li_3(NH_2)_2I$ [28], the ^7Li spin-lattice relaxation rate maximum at 14 MHz was found near 310 K, and the step-like narrowing of the ^7Li NMR line was observed near 220 K. While the PFG-NMR results are consistent with high Li^+ diffusivity in $Li_3(NH_2)_2I$, the activation energy obtained from the PFG-NMR data appears to be lower than that derived from fitting of the ^7Li spin-lattice relaxation data (380 meV over the range of 228–401 K [28]). Thus, the basis for comparison between the values of D and τ^{-1} for $Li_3(NH_2)_2I$ is not so well established, as in the case of $LiLa(BH_4)_3Cl$. For such a comparison, it is reasonable to choose the temperature of the ^7Li spin-lattice relaxation rate maximum for $Li_3(NH_2)_2I$ (310 K at 14 MHz [28]), since at this temperature, the estimate of τ^{-1} (8.8×10^7 s^{-1}) is the most reliable. The extrapolation of the Li^+ diffusivity data gives $D(310K) \approx 7.8 \times 10^{-9}$ cm^2/s, and, neglecting any correlations, for the average jump length L, we obtain 2.3 Å.

In the hexagonal crystal structure of $Li_3(NH_2)_2I$ [6], two inequivalent Li sites (Li1 and Li2) form alternating layers perpendicular to the c axis; see Fig. 4. The sublattice of Li sites is characterized by rather short Li – Li distances. Each Li1 atom has two Li1 nearest neighbors (in the same layer) at a distance of 2.28 Å and one Li2 nearest neighbor (in the adjacent layer) at a distance of 2.39 Å. Each Li2 has one Li1 nearest neighbor (in the adjacent layer) at a distance of 2.39 Å and two Li2 nearest neighbors (in the same layer) at a distance of 2.84 Å. According to the structural results [6], both Li1 and Li2 sites are fully occupied; therefore, interstitial sites in the lattice may play an important role for Li^+ diffusion. Possible diffusion paths (see Fig. 4) were analyzed [29] using the program TOPOS [42]. The analysis has revealed three types of large interstitial sites (2*b*, $6c_1$ and $6c_2$) located slightly off the Li layers (Fig. 4); the effective radii of these voids are in the range 1.58–1.70 Å. These interstitial sites form the three-dimensional network of channels

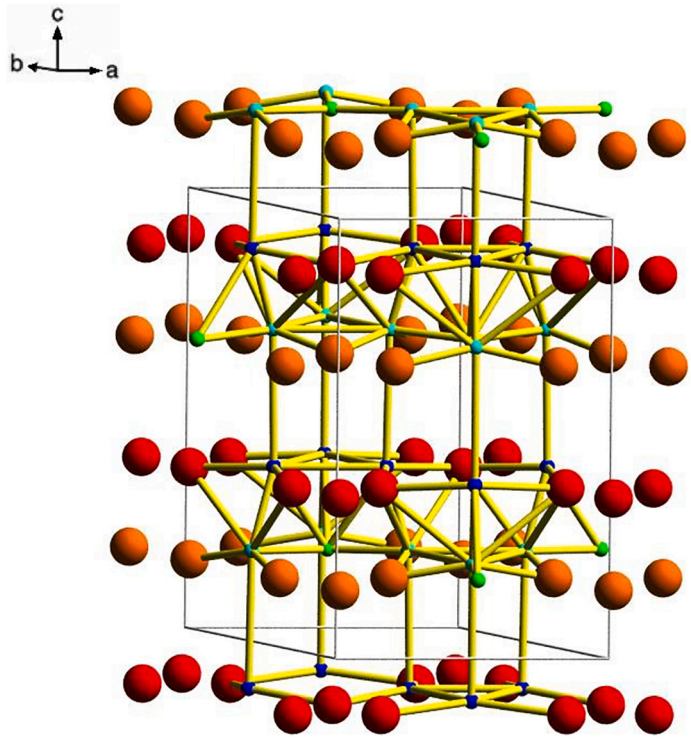

Fig. 4. The sublattice of Li sites in $Li_3(NH_2)_2I$ and the network of channels for Li^+ diffusion. Red spheres: Li1 sites; orange spheres: Li2 sites; green spheres: 2*b* interstitial sites; dark blue spheres: $6c_1$ interstitial sites; light blue spheres: $6c_2$ interstitial sites. Yellow bars show the possible diffusion paths. (For interpretation of the references to colour in this figure legend, the reader is referred to the web version of this article.)

shown in Fig. 4. The nearest-neighbor distances within this network are in the range from 2.22 Å to 3.11 Å; the shortest distances correspond to Li2 – $6c_2$ (2.22 Å), $6c_1$ – $6c_2$ (2.25 Å), 2*b* – $6c_2$ (2.35 Å), and Li1 – $6c_1$ (2.62 Å). Thus, the above estimate of the average jump length *L* appears to be consistent with the proposed diffusion paths. According to the previous NMR studies [28], high Li^+ mobility in $Li_3(NH_2)_2I$ cannot be related to the effects of NH_2 reorientations, since no signs of reorientational motion of NH_2 groups were found at the frequency scale of Li^+ jump rate.

Using the density of charge carriers in $Li_3(NH_2)_2I$ ($n = 2.39 \times 10^{22}$ cm^{-3} [28]) and the extrapolated value of the Li^+ diffusivity $D(310\ K) \approx 7.8 \times 10^{-9}$ cm^2/s, from the Nernst-Einstein equation we obtain $\sigma(310\ K) \approx 1.4 \times 10^{-3}$ S/cm. The measured conductivity of $Li_3(NH_2)_2I$ is considerably lower ($\sim 3 \times 10^{-5}$ S/cm near 310 K [6]). It should be noted, however, that the conductivity measurements [6] were performed on pellets containing the additional $LiNH_2$ phase with very low conductivity; this is expected to reduce the measured conductivity with respect to the pure $Li_3(NH_2)_2I$ compound. The activation energy for the Li^+ diffusion coefficient derived from our present experiments (224 meV) is lower than that for the measured conductivity ($\sim$ 580 meV over the range of 300–425 K [6]). Similar discrepancies are often observed for various compounds; in particular, they are typical of nanocrystalline ionic conductors [43]. Presumably, such discrepancies may be attributed to the effects of large-scale inhomogeneities (such as grain boundaries), since the diffusivity and the conductivity are generally measured on different spatial scales. Although our $Li_3(NH_2)_2I$ sample is prepared by ball milling, after the annealing at 423 K (see Section 2), it is no longer nanocrystalline. In fact, according to X-ray diffraction analysis [6], the crystallite sizes of the annealed $Li_3(NH_2)_2I$ sample are at least several hundred nanometers, i.e., they are more than a few times 10^{-5} cm. The mean-square displacement $\langle r^2 \rangle$ of Li^+ ions in the course of our diffusivity measurements can be estimated as $\langle r^2 \rangle = 6Dt$, where *t* is the characteristic diffusion time. Taking a typical diffusion time of 10 ms and $D(343\ K) \approx 1.7 \times 10^{-8}$ cm^2/s for $Li_3(NH_2)_2I$, we obtain $\langle r^2 \rangle \approx 10^{-9}$ cm^2, i.e., $\langle r^2 \rangle^{1/2} \approx 3.2 \times 10^{-5}$ cm. This gives the spatial scale over which the diffusion coefficients are probed in our experiments.

3.3. Li^+ diffusivity in $LiCB_9H_{10}$

The evolution of the measured ^7Li NMR spectra with temperature for $LiCB_9H_{10}$ is presented in Fig. S3 of the Supplementary Information. Fig. 5 shows the temperature dependence of the ^7Li NMR line width Δ_{Li} (full width at half-maximum) for $LiCB_9H_{10}$ measured at 28 MHz. The observed behavior of Δ_{Li} is typical of systems exhibiting thermally activated diffusion of Li^+ ions. Below 240 K, the line width is nearly constant, being determined by static dipole-dipole and quadrupole interactions of ^7Li nuclei. The motional narrowing of the spectrum occurs, when the Li^+ jump rate becomes comparable to the "rigid-lattice" line

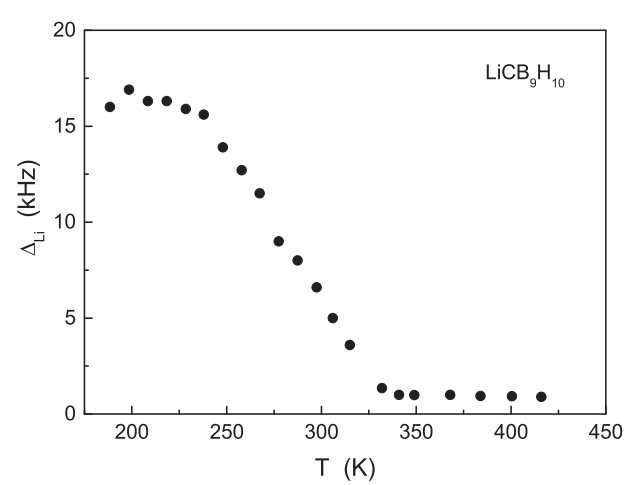

Fig. 5. Temperature dependence of the width (full width at half-maximum) of the ^7Li NMR spectrum for $LiCB_9H_{10}$.

width (~10^4 s^{-1}). Above 340 K, the value of Δ_{Li} is very small (< 1 kHz); this indicates that the observed line narrowing is related to the *long-range* diffusion of Li^+ ions. It is interesting to note that, since the two-stage order-disorder phase transition in $LiCB_9H_10$ occurs in the range 330–350 K [10], the ^{7}Li line narrowing is nearly complete already in the ordered (low-temperature) phase.

The behavior of the Li^+ diffusivity in $LiCB_9H_{10}$ resulting from our PFG-NMR measurements is shown in Fig. 6. The measured diffusion coefficients for $LiCB_9H_{10}$ are an order-of-magnitude higher than those for both $LiLa(BH_4)_3Cl$ and $Li_3(NH_2)_2I$ in the same temperature range (cf. Figs. 6 and 2). This is consistent with the extremely high Li-ion conductivity in the disordered phase of $LiCB_9H_{10}$ [10]. As can be seen from Fig. 6, in the temperature range 360–403 K (where $LiCB_9H_{10}$ exists as the orientationally-disordered hexagonal phase [10]), the Li^+ diffusivity is well described by the Arrhenius law. The activation energy for Li-ion diffusion derived from the Arrhenius fit in this temperature range is 265 (6) meV. The significant drop of the diffusivity below 360 K can be related to the order-disorder phase transition. This is consistent with the sharp drop of the ionic conductivity of $LiCB_9H_{10}$ observed in the same range [10]. Included in Fig. 6 are also the results of PFG-NMR measurements of Li^+ diffusivity for the mixed-anion solid solution $Li(CB_9H_{10})_{0.7}(CB_{11}H_{12})_{0.3}$ [25]. For this compound, the order-disorder phase transition is suppressed, so that at room temperature it retains the same basic structure as the high-*T* (disordered) phase of $LiCB_9H_{10}$ [10]. It should be noted that our values of Li^+ diffusivity for the disordered phase of $LiCB_9H_{10}$ appear to be close to the extrapolation of the *D* (*T*) results for $Li(CB_9H_{10})_{0.7}(CB_{11}H_{12})_{0.3}$ (see Fig. 6).

The Li^+ jump rate in the disordered phase of $LiCB_9H_{10}$ cannot be reliably estimated from the ^{7}Li spin-lattice relaxation data [10], since the relaxation rate maximum is not observed for this phase. On the basis of the ^{7}Li spin-lattice relaxation results [10], we can only conclude that above 360 K, the Li^+ jump rate exceeds 10^8 s^{-1}. Thus, a comparison between the diffusivity and spin-lattice relaxation data cannot be used to estimate the average jump length for $LiCB_9H_{10}$. However, we can compare the diffusivity and conductivity results on the basis of the Nernst-Einstein equation. The activation energy for conductivity in the high-temperature phase of $LiCB_9H_{10}$ estimated over the range of ~353–383 K is approximately 290 meV [10]. Taking into account the narrow temperature range, this value appears to be consistent with our experimental value for Li^+ diffusivity in the high-temperature phase, 265(6) meV. Using the structural data for this phase at 383 K [10], we obtain the charge carrier density $n = 4.61 \times 10^{21}$ cm^{-3}, and Eq. (3) with our diffusivity value of $D(383\ K) = 1.26 \times 10^{-6}$ cm^2/s yields the conductivity of 2.8×10^{-2} S/cm. The measured conductivity of $LiCB_9H_{10}$ at 383 K is approximately 8×10^{-2} S/cm [10], i. e., nearly a factor of three higher than that estimated from the Nernst-Einstein equation. This means that the Haven ratio H_R [44] for $LiCB_9H_{10}$ is about 0.35. The values of $H_R < 1$ in fast ionic conductors are usually related to ion-ion interactive effects [44]. It should be noted that similar observations (the measured conductivity exceeding that estimated from the tracer diffusivity results) were also reported for the related mixed-anion solid solution $Li(CB_9H_{10})_{0.7}(CB_{11}H_{12})_{0.3}$ [25] and tentatively attributed to strong correlations between diffusing cations [45,46]. Recent ab initio molecular dynamics calculations [46] have revealed the importance of the concerted migration of multiple ions in a number of superionic conductors. The concerted-migration mechanism is shown to lead to a considerable decrease in the effective energy barriers with respect to the barriers for individual ion jumps [46].

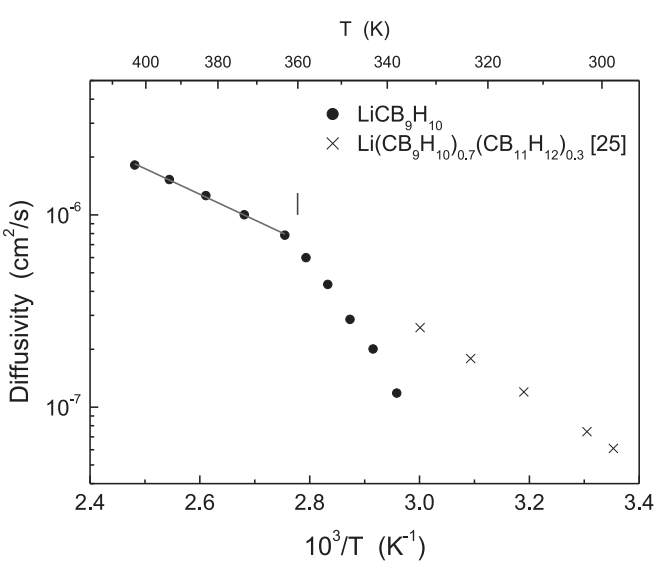

Fig. 6. The measured Li^+ diffusion coefficient for $LiCB_9H_{10}$ as a function of the inverse temperature. The red line shows the Arrhenius fit to the data in the range 363–403 K. The vertical blue bar indicates the phase boundary for the disordered high-*T* phase of $LiCB_9H_{10}$. For comparison, the measured Li^+ diffusion coefficients for the mixed-anion $Li(CB_9H_{10})_{0.7}(CB_{11}H_{12})_{0.3}$ from Ref. [25] are shown by crosses. (For interpretation of the references to colour in this figure legend, the reader is referred to the web version of this article.)

4. Conclusions

Our pulsed-field-gradient spin-echo experiments have revealed fast Li^+ diffusivities in the complex hydrides $LiLa(BH_4)_3Cl$, $Li_3(NH_2)_2I$, and $LiCB_9H_{10}$. At 400 K, the measured diffusion coefficients exceed 10^{-7} cm^2/s for $LiLa(BH_4)_3Cl$, 5×10^{-8} cm^2/s for $Li_3(NH_2)_2I$, and 10^{-6} cm^2/s for $LiCB_9H_{10}$. For $LiLa(BH_4)_3Cl$ and $Li_3(NH_2)_2I$, the diffusion coefficients are found to follow Arrhenius behaviors over the entire temperature ranges studied, with the activation energies of 268(6) meV and 224(6) meV, respectively. For $LiCB_9H_{10}$, an Arrhenius behavior with the activation energy of 265(6) meV is observed in the disordered high-*T* phase (360–403 K), whereas below 360 K, the measured diffusivity drops significantly due to the transition to the ordered phase. It is interesting to note that, for all the studied complex hydrides, the activation energies for Li^+ diffusion are in the same range of ~220–270 meV. These small values of the activation energies may be related to high Li^+ mobilities; indeed, for all the studied compounds, the jump rates of Li ions are of the order of 10^8 s^{-1} near room temperature.

For $LiLa(BH_4)_3Cl$, the activation energy for the Li-ion diffusion coefficient is in reasonable agreement with that for the Li^+ jump rate, as derived from the ^{7}Li spin-lattice relaxation rate measurements. Comparison of the PFG-NMR results with the ^{7}Li spin-lattice relaxation data supports the diffusion mechanism, including Li^+ jumps between 12*d* and 6*b* interstitial sites in the cubic lattice of $LiLa(BH_4)_3Cl$. Furthermore, the room-temperature ionic conductivity estimated from the diffusivity data on the basis of Nernst-Einstein equation is consistent with the measured room-temperature conductivity value.

For $Li_3(NH_2)_2I$, the measured activation energy for the Li-ion diffusion coefficient appears to be lower than the activation energies for both the conductivity and the Li^+ jump rate. Thus, the basis for comparison of the PFG-NMR results with the ^{7}Li spin-lattice relaxation data for $Li_3(NH_2)_2I$ is not so well established, as in the case of $LiLa(BH_4)_3Cl$. However, a rough estimate of the elementary jump length in $Li_3(NH_2)_2I$ at 310 K gives the value of 2.3 Å, which is consistent with the diffusion mechanism proposed in our previous works.

For the disordered phase of $LiCB_9H_{10}$, the activation energy for the Li-ion diffusion coefficient is close to that for the ionic conductivity; however, the measured conductivity is about a factor of three higher than that estimated from the Nernst-Einstein equation. This feature is believed to originate from strongly correlated cation motion in *closo*-hydroborates.

Declaration of Competing Interest

The authors declare that they have no known competing financial interests or personal relationships that could have appeared to influence the work reported in this paper.

Acknowledgments

This work was supported by the Russian Science Foundation (Grant. No. 19-12-00009). We are also grateful to Independent research fund Denmark (DFF-9041-00226B and DFF-4181-00462) and JSPS KAKENHI, Hydrogenomics (JP18H05513).

Appendix A. Supplementary data

Examples of the spin-echo attenuation data for $LiLa(BH_4)_3Cl$ and $Li_3(NH_2)_2I$, the evolution of the measured ^7Li NMR spectra with temperature for $LiCB_9H_{10}$, and exemplary ^1H NMR spectra. Supplementary data to this article can be found online at https://doi.org/10.1016/j.ssi.2021.115585.

References

[1] S. Orimo, Y. Nakamori, J.R. Elisen, A. Züttel, C.M. Jensen, Complex hydrides for hydrogen storage, Chem. Rev. 107 (2007) 4111–4132.

[2] M. Paskevicius, L. Jepsen, P. Schouwink, R. Černý, D.B. Ravnsbæk, Y. Filinchuk, M. Dornheim, F. Besenbacher, T.R. Jensen, Metal borohydrides and derivatives – synthesis, structure and properties, Chem. Soc. Rev. 46 (2017) 1565–1634.

[3] M. Matsuo, Y. Nakamori, S. Orimo, H. Maekawa, H. Takamura, Lithium superionic conduction in lithium borohydride accompanied by structural transition, Appl. Phys. Lett. 91 (2007) 224103.

[4] H. Maekawa, M. Matsuo, H. Takamura, M. Ando, Y. Noda, T. Karahashi, S. Orimo, Halide-stabilized $LiBH_4$, a room-temperature lithium fast-ion conductor, J. Am. Chem. Soc. 131 (2009) 894–895.

[5] M. Matsuo, A. Remhof, P. Martelli, R. Caputo, M. Ernst, Y. Miura, T. Sato, H. Oguchi, H. Maekawa, H. Takamura, A. Borgschulte, A. Züttel, S. Orimo, Complex hydrides with $(BH_4)^-$ and $(NH_2)^-$ anions as new lithium fast-ion conductors, J. Am. Chem. Soc. 131 (2009) 16389–16391.

[6] M. Matsuo, T. Sato, Y. Miura, H. Oguchi, Y. Zhou, H. Maekawa, H. Takamura, S. Orimo, Synthesis and lithium fast-ion conductivity of a new complex hydride $Li_3(NH_2)_2I$ with double-layered structure, Chem. Mater. 22 (2010) 2702–2704.

[7] M.B. Ley, S. Boulineau, R. Janot, Y. Filinchuk, T.R. Jensen, New Li-ion conductors and solid state hydrogen storage materials: $LiM(BH_4)_3Cl$, M = La, Gd, J. Phys. Chem. C 116 (2012) 21267–21276.

[8] T.J. Udovic, M. Matsuo, A. Unemoto, N. Verdal, V. Stavila, A.V. Skripov, J.J. Rush, H. Takamura, S. Orimo, Sodium superionic conduction in $Na_2B_{12}H_{12}$, Chem. Commun. 50 (2014) 3750–3752.

[9] T.J. Udovic, M. Matsuo, W.S. Tang, H. Wu, V. Stavila, A.V. Soloninin, R. V. Skoryunov, O.A. Babanova, A.V. Skripov, J.J. Rush, A. Unemoto, H. Takamura, S. Orimo, Exceptional superionic conductivity in disordered sodium decahydro-*closo*-decaborate, Adv. Mater. 26 (2014) 7622–7626.

[10] W.S. Tang, M. Matsuo, H. Wu, V. Stavila, W. Zhou, A.A. Talin, A.V. Soloninin, R. V. Skoryunov, O.A. Babanova, A.V. Skripov, A. Unemoto, S. Orimo, T.J. Udovic, Liquid-like ionic conduction in solid lithium and sodium monocarba-*closo*-decaborates near or at room temperature, Adv. Energy Mater. 6 (2016) 1502237.

[11] W.S. Tang, K. Yoshida, A.V. Soloninin, R.V. Skoryunov, O.A. Babanova, A. V. Skripov, M. Dimitrievska, V. Stavila, S. Orimo, T.J. Udovic, Stabilizing superionic-conducting structures via mixed-anion solid solutions of monocarba-*closo*-borate salts, ACS Energy Lett. 1 (2016) 659–664.

[12] T. Tsang, T.C. Farrar, Nuclear magnetic resonance studies of internal rotations and phase transitions in borohydrides of lithium, sodium, and potassium, J. Chem. Phys. 50 (1969) 3498–3502.

[13] A.V. Skripov, O.A. Babanova, A.V. Soloninin, V. Stavila, N. Verdal, T.J. Udovic, J. J. Rush, Nuclear magnetic resonance study of atomic motion in $A_2B_{12}H_{12}$ (A = Na, K, Rb, Cs): anion reorientations and Na^+ mobility, J. Phys. Chem. C 117 (2013) 25961–25968.

[14] A.V. Skripov, A.V. Soloninin, O.A. Babanova, R.V. Skoryunov, Nuclear magnetic resonance studies of atomic motion in borohydride-based materials: fast anion reorientations and cation diffusion, J. Alloys Compd. 645 (2015) S428–S433.

[15] A.V. Skripov, A.V. Soloninin, O.A. Babanova, R.V. Skoryunov, Anion and cation dynamics in polyhydroborate salts: NMR studies, Molecules 25 (2020) 2940.

[16] Z. Lu, F. Ciucci, Structural origin of the superionic Na conduction in $Na_2B_{10}H_{10}$ *closo*-borates and enhanced conductivity by Na deficiency for high performance solid electrolyte, J. Mater. Chem. A 4 (2016) 17740–17748.

[17] J.B. Varley, K. Kweon, P. Mehta, P. Shea, T.W. Heo, T.J. Udovic, V. Stavila, B. C. Wood, Understanding ionic conductivity trends in polyborane solid electrolytes from *ab initio* molecular dynamics, ACS Energy Lett. 2 (2017) 250–255.

[18] K. Kweon, J.B. Varley, P. Shea, N. Adelstein, P. Mehta, T.W. Heo, T.J. Udovic, V. Stavila, B.C. Wood, Structural, chemical, and dynamical frustration: origins of superionic conductivity in *closo*-borate solid electrolytes, Chem. Mater. 29 (2017) 9142–9153.

[19] M. Dimitrievska, P. Shea, K.E. Kweon, M. Bercx, J.B. Varley, W.S. Tang, A. V. Skripov, V. Stavila, T.J. Udovic, B.C. Wood, Carbon incorporation and anion dynamics as synergistic drivers for ultrafast diffusion in superionic $LiCB_{11}H_{12}$ and $NaCB_{11}H_{12}$, Adv. Energy Mater. 6 (2018) 1703422.

[20] O.A. Babanova, A.V. Soloninin, A.P. Stepanov, A.V. Skripov, Y. Filinchuk, Structural and dynamical properties of $NaBH_4$ and KBH_4: NMR and synchrotron X-ray diffraction studies, J. Phys. Chem. C 114 (2010) 3712–3718.

[21] E.O. Stejskal, J.E. Tanner, Spin diffusion measurements: spin echos in the presence of a time-dependent field gradient, J. Chem. Phys. 42 (1965) 288–292.

[22] P. Stilbs, Fourier transform pulsed-gradient spin-echo studies of molecular diffusion, Progr. Nucl. Magn. Res. Spectr. 19 (1987) 1–45.

[23] W.S. Price, NMR Studies of Translational Motion – Principles and Applications, University Press, Cambridge, UK, 2009.

[24] P.T. Callaghan, Translational Dynamics and Magnetic Resonance – Principles of Pulsed Gradient Spin Echo NMR, University Press, Oxford, UK, 2011.

[25] S. Kim, H. Oguchi, N. Toyama, T. Sato, S. Takagi, T. Otomo, D. Arunkumar, N. Kuwata, J. Kawamura, S. Orimo, A complex hydride lithium superionic conductor for high-energy-density all-solid-state lithium metal batteries, Nat. Commun. 10 (2019) 1081.

[26] A.V. Skripov, G. Majer, O.A. Babanova, R.V. Skoryunov, A.V. Soloninin, M. Dimitrievska, T.J. Udovic, Na^+ diffusivity in carbon-substituted *nido*- and *closo*-hydroborate salts: pulsed-field-gradient NMR studies of Na-7-$CB_{10}H_{13}$ and $Na_2(CB_9H_{10})(CB_{11}H_{12})$, J. Alloys Compd. 850 (2021) 156781.

[27] A.V. Skripov, A.V. Soloninin, M.B. Ley, T.R. Jensen, Y. Filinchuk, Nuclear magnetic resonance study of BH_4 reorientations and Li diffusion in $LiLa(BH_4)_3Cl$, J. Phys. Chem. C 117 (2013) 14965–14972.

[28] A.V. Skripov, R.V. Skoryunov, A.V. Soloninin, O.A. Babanova, M. Matsuo, S. Orimo, Atomic motion in the complex hydride $Li_3(NH_2)_2I$: ^7Li and ^1H nuclear magnetic resonance studies, J. Phys. Chem. C 119 (2015) 13459–13464.

[29] A.V. Skripov, K. Volgmann, C.V. Chandran, R.V. Skoryunov, O.A. Babanova, A. V. Soloninin, S. Orimo, P. Heitjans, NMR studies of lithium diffusion in $Li_3(NH_2)_2I$ over wide range of Li^+ jump rates, Z. Phys. Chem. 231 (2017) 1455–1465.

[30] A.V. Soloninin, M. Dimitrievska, R.V. Skoryunov, O.A. Babanova, A.V. Skripov, W. S. Tang, V. Stavila, S. Orimo, T.J. Udovic, Comparison of anion reorientational dynamics in MCB_9H_{10} and $M_2B_{10}H_{10}$ (M = Li, Na) via nuclear magnetic resonance and quasielastic neutron scattering studies, J. Phys. Chem. C 121 (2017) 1000–1012.

[31] The mention of all commercial suppliers in this paper is for clarity and does not imply the recommendation or endorsement of these suppliers by NIST.

[32] J.E. Tanner, Use of the stimulated echo in NMR diffusion studies, J. Chem. Phys. 52 (1970) 2523–2526.

[33] W.S. Price, P. Kuchel, Effect of nonrectangular field gradient pulses in the Stejskal and Tanner (diffusion) pulse sequence, J. Magn. Reson. 94 (1991) 133–139.

[34] G. Majer, K. Zick, Accurate and absolute diffusion measurements of rhodamine 6G in low-concentration aqueous solutions by the PGSE-WATERGATE sequence, J. Chem. Phys. 142 (2015) 164202.

[35] Y.-S. Lee, M.B. Ley, T.R. Jensen, Y.W. Cho, Lithium ion disorder and conduction mechanism in $LiCe(BH_4)_3Cl$, J. Phys. Chem. C 120 (2016) 19035–19042.

[36] C. Frommen, M.H. Sørby, P. Ravindran, P. Vajeeston, H. Fjelvåg, B.C. Hauback, Synthesis, crystal structure, and thermal properties of the first mixed-metal and anion-substituted rare earth borohydride $LiCe(BH_4)_3Cl$, J. Phys. Chem. C 115 (2011) 23591–23602.

[37] M.B. Ley, D.B. Ravnsbæk, Y. Filinchuk, Y.-S. Lee, R. Janot, Y.W. Cho, J. Skibsted, T. R. Jensen, $LiCe(BH_4)_3Cl$, a new lithium-ion conductor and hydrogen storage material with isolated tetranuclear anionic clusters, Chem. Mater. 24 (2012) 1654–1663.

[38] H.W. Spiess, Deuteron spin-alignment: a probe for studying ultraslow motions in solids and solid polymers, J. Chem. Phys. 72 (1980) 6755–6762.

[39] M. Wilkening, P. Heitjans, New prospects in studying Li diffusion – two-time stimulated echo NMR of spin-3/2 nuclei, Solid State Ionics 177 (2006) 3031–3036.

[40] M. Wilkening, P. Heitjans, From micro to macro: access to long-range Li^+ diffusion parameters in solids via microscopic $^{6,7}Li$ spin-alignment echo NMR spectroscopy, ChemPhysChem 13 (2012) 53–65.

[41] S.P. GharibDoust, M. Brighi, Y. Sadikin, D.B. Ravnsbæk, R. Černý, J. Skibsted, T. R. Jensen, Synthesis, structure and Li-ion conductivity of $LiLa(BH_4)_3X$, X = Cl, Br, I, J. Phys. Chem. C 121 (2017) 19010–19021.

[42] V.A. Blatov, A.P. Shevchenko, D.M. Proserpio, Applied topological analysis of crystal structures with the program package ToposPro, Cryst. Growth Des. 14 (2014) 3576–3586.

[43] P. Heitjans, S. Indris, Diffusion and ionic conduction in nanocrystalline ceramics, J. Phys. Condens. Matter 15 (2003) R1257–R1289.

[44] G.E. Murch, The Haven ratio in fast ionic conductors, Solid State Ionics 7 (1982) 177–198.

[45] H. Okazaki, Deviation from the Einstein relation in average crystals self-diffusion of Ag^+ ions in α-Ag_2S and α-Ag_2Se, J. Phys. Soc. Jpn. 23 (1967) 355–360.

[46] X. He, Y. Zhu, Y. Mo, Origin of fast ion diffusion in super-ionic conductors, Nat. Commun. 8 (2017) 15893.